Total Body PET: Why, How, What for?

Suleman Surti, *Senior Member, IEEE*, Austin R. Pantel, and Joel S. Karp, *Life Fellow, IEEE*

Abstract—PET instruments are now available with a long axial field-of-view (LAFOV) to enable imaging the total-body, or at least head and torso, simultaneously and without bed translation. This has two major benefits, a dramatic increase in system sensitivity and the ability to measure kinetics with wider axial coverage so as to include multiple organs. This article presents a review of the technology leading up to the introduction of these new instruments, and explains the benefits of an LAFOV PET-CT instrument. To date there are two platforms developed for total-body PET (TB-PET), an outcome of the EXPLORER Consortium of the University of California at Davis (UC Davis) and the University of Pennsylvania (Penn). The uEXPLORER at UC Davis has an AFOV of 194 cm and was developed by United Imaging Healthcare. The PennPET EXPLORER was developed at Penn and is based on the digital detector from Philips Healthcare. This multiring system is scalable and has been tested with 3 rings but is now being expanded to 6 rings for 140 cm. Initial human studies with both EXPLORER systems have demonstrated the successful implementation and benefits of LAFOV scanners for both clinical and research applications. Examples of such studies are described in this article.

Index Terms—Long axial-field-of-view (LAFOV), PennPET EXPLORER, PET-CT, total-body PET (TB-PET), uEXPLORER.

I. INTRODUCTION

SINCE the earliest positron tomographs were built in the mid-1970's there have been significant advancements in the technology, such that the performance of today's commercial PET-CT instruments is outstanding. Whole-body PET imaging has been in standard clinical practice for several decades, and total-body (TB) biodistribution studies are routinely performed to evaluate new radio-tracers. But it is important to understand that the design of these systems is targeted toward the primary clinical applications and characteristics of the radiotracer used for these studies, and that whole-body surveys require bed translation. It is well known that ^{18}F-Fluorodeoxyglucose (FDG), a marker of glycolysis, is the most widely used PET tracer for cancer diagnosis and staging [1]. There are, though, other

fluorinated radio-tracers becoming more routinely available, such as ^{18}F-florbetapir, ^{18}F-florbetaben, and ^{18}F-flutemetamol to detect amyloid in suspected Alzheimer's disease [2] and ^{18}F-fluciclovine (Axumin) to detect sites of disease in men with biochemical recurrence of prostate cancer [3]. In addition, there are also radioisotopes that require generators and are used in the clinic, such as, for example, ^{82}Rb for a myocardial perfusion stress test and ^{68}Ga-DOTATATE for imaging neuroendocrine tumors. Given the current status of clinical PET one might ask whether the needs are adequately served by the current capabilities of today's commercial instruments, which can achieve excellent diagnostic quality for an FDG scan of 10–15 min (or less, depending on the patient size) with a dose of 10–15 mCi (370–555 MBq). Do we need a long axial field-of-view (LAFOV) PET scanner to improve clinical imaging, reduce patient dose, or increase patient throughput—or will the main role of such an instrument be to study the biodistribution of new radio-tracers and enable research investigations that require a large axial coverage? The benefits of an LAFOV PET scanner will be discussed in a later section, but stem mainly from the increase in sensitivity and ability to dynamically study multiorgan systems. Early human studies on LAFOV instruments suggest the enormous potential of TB PET and examples are given in a later section to highlight areas of opportunity for both clinical and research applications. In this introduction, we first provide a brief overview of the technology of clinical PET systems to give perspective to the development of total-body PET (TB-PET) systems that is now taking place, since many of the established concepts for PET scanners with a standard (clinical) AFOV are relevant for LAFOV PET scanners, as well. In the second part of this article different parameters concerning the design of LAFOV PET scanners (axial length, detector design components and geometry, system design) are discussed. Finally, we end with a description of some of the clinical and research studies that are enabled with the LAFOV PET systems.

Early PET scanners were originally based on NaI(Tl) scintillators but transitioned in the early 1980's to multiring systems with bismuth germanate (BGO) crystals due to the higher stopping efficiency of BGO for 511 keV photons [4]. A major innovation was to couple a small group of photomultiplier tubes (PMTs) in a light sharing "block" design [5]. This detector design produced good spatial resolution in combination with the high sensitivity of BGO. However, poor energy resolution required the use of axial septa (or collimation in the axial direction) to limit the acquisition of scattered (within object) events which add bias to the reconstructed image unless properly corrected. This mode of data acquisition in direct slices (2-D mode) while reducing scatter events significantly limited the overall sensitivity of the PET system. Hence,

these systems traded off geometric system sensitivity for high intrinsic detector efficiency.

Starting in mid-1970s there was a parallel effort in developing PET scanners operating in fully 3-D mode, i.e., without any septa, to maximize overall sensitivity [6], [7]. The early 1990s saw the commercialization of NaI(Tl)-based whole-body PET scanners that were targeted for FDG imaging and were 25 cm long axially [8], [9]. These systems used large continuous NaI(Tl) crystals in an Anger-logic detector design to provide not only good spatial resolution but also good energy resolution that helps limit collection of scatter events. Operating in fully 3D mode with longer AFOV, these systems had much higher geometric sensitivity than 2-D BGO scanners, however, the lower intrinsic sensitivity of NaI(Tl) limited the overall system sensitivity and versatility of these systems.

There was also a significant effort put in developing TOF PET scanners that started in the late-1970s though early 1980s [10]. Due to the long decay times of BGO and NaI(Tl), neither of these crystals provided adequate timing resolution to be utilized in time-of-flight (TOF) PET systems. The fast scintillators available at that time (BaF_2 and CsF) that were used for TOF PET, however, had low sensitivity and also low light output which led to poor spatial and energy resolution. Hence, they operated in 2-D mode with septa further impacting system sensitivity. While TOF-assisted reconstruction was useful for improving image signal-to-noise properties [11], [12], these systems had lower overall sensitivity, as well as worse spatial resolution.

Development of new Lu-based scintillators [13] in the late 1990s and early 2000s led to LSO and LYSO crystals that have a high stopping efficiency for 511 keV photons (close to BGO), while also being fast enough to allow very good coincidence timing resolution (CTR). The high light output of these crystals not only helped achieve excellent CTR but also enabled improved spatial resolution and ability to operate in fully 3-D mode that maximizes system sensitivity. Hence, starting in 2006 a new generation of fully 3-D TOF PET commercial scanners with very high sensitivity, now all PET/CT, were developed [14]. These systems, and those from other vendors that quickly followed, utilized light sharing detector designs using small pixels of Lu-based crystals to achieve high spatial resolution (4–5 mm) with 25 to 39-mm diameter PMTs. The CTR of these scanners lies within the range of 450–600 ps—very similar to the scanners developed in the 1980s, but with superior spatial resolution and sensitivity [15]. While NaI(Tl)-based scanners were phased out in the early 2000's, BGO-based scanners continued to be marketed until very recently since they were a very cost-effective means to achieve high spatial resolution and high sensitivity. While BGO systems could not offer TOF, they were shown in the 1990's to be capable of 3-D imaging without septa [16], [17].

More recent progress in photosensor technology has led to the development of digital PET/CT scanners from all major PET manufacturers, utilizing silicon photo-multipliers (SiPMs) instead of the traditional PMTs [18]–[20]. Compactness and flexibility of SiPMs provides improved PET detector designs with greatly reduced signal multiplexing (number of crystal relative to photosensor channels) and improved light

collection. This, in turn, has led to some improvements in spatial resolution and much larger gains in the system CTR. These digital PET/CT systems all utilize 19–25 mm thick lutetium-based scintillators that provide very high detection sensitivity and operate in fully 3-D mode. Iterative image reconstruction, combined with CT attenuation correction, model-based scatter correction, and TOF leads to quantitative images with a high signal-to-noise ratio. Currently, four commercial manufacturers offer whole-body TOF PET scanners: Siemens with the Biograph mCT (21.6 cm) and Biograph Vision (26.3 cm), GE with the Discovery MI (20 cm and 25 cm), United Imaging with the uMI 550 (24 cm) and uMI 780 (30 cm), and Canon (formerly Toshiba) with the Celestion (19.6 cm) and Cartesion Prime (25 cm). Geared toward oncologic FDG studies, these digital PET/CT systems can perform whole-body surveys in 10–15 min with excellent image quality for both heavy and light patients due to the improved sensitivity and CTR.

Despite the high detector sensitivity (63%–77% detection probability for coincident 511 keV gammas) and fully 3-D data acquisition, the absolute sensitivity of these new digital systems is limited by the axial length (15–30 cm): 5%–11% for a point source placed at the center of the scanner, or 0.6%–2% (or 6–20 kcps/MBq) as specified by the 70-cm long NEMA line source measurement. Improved system sensitivity would allow for further reductions in injected dose and scan time, imaging of new radioisotopes with reduced flux, and for dynamic imaging where short time frames are required to capture the fast kinetics but the statistical uncertainties of the data can lead to errors in biologic parameter estimation. Further, the modest axial length of commercial PET scanners limits our ability to observe temporal changes in the tracer kinetics to a single organ, which has been shown to be important in monitoring the progression of disease. In contrast, an LAFOV PET system would allow simultaneous dynamic imaging of multiple organs, thereby enabling the study of disease affecting multiple organ systems.

II. DEVELOPMENT OF LAFOV TB-PET SYSTEMS

A. Thicker Crystals or Longer AFOV for Increased Sensitivity?

PET system sensitivity can be increased by using thicker crystals, increasing the axial length and/or reducing ring diameter [21]. While ring diameter can be reduced, any significant reduction can limit the patient population or increase claustrophobia. Here, axial length and crystal thickness are the two main factors considered in determining system sensitivity. In Fig. 1, we show calculations for point source in air sensitivity as a function of crystal thickness and varying scanner axial length. As shown, there is a diminishing gain in sensitivity as the crystal thickness is increased beyond 30 mm, especially for scanner with shorter axial length. For example, in a 25-cm long scanner, increasing the crystal thickness from 20 mm to 50 mm (increase of 2.5 in crystal volume) leads to a gain in sensitivity from 6.5% to 12.8%. Instead, if the scanner axial length is increased to 62.5 cm while keeping the crystal thickness at 20 mm (same increase of 2.5 in crystal volume) the sensitivity increases to 14.4%. In fact, a prior study has shown that for a fixed crystal volume one can
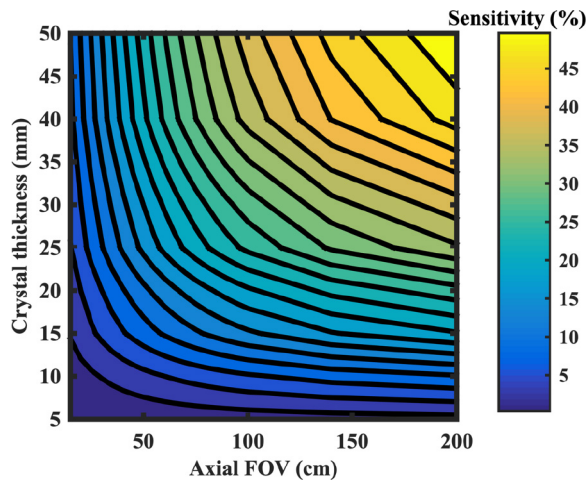
Fig. 1. Contour plot of the percent sensitivity of a point source in air as a function of crystal thickness and scanner axial length. The detector ring diameter was fixed at 85 cm and LSO was used as the scintillator material.

TABLE I
RELATIVE SENSITIVITY FOR SELECTED SCANNER AXIAL LENGTHS AS CALCULATED FOR THREE DIFFERENT IMAGING SETUPS. THE PHANTOMS ARE 200 cm LONG CYLINDERS

Scanner AFOV (cm)	20	70	100	140	200
Point source in air placed at the center of AFOV (A)	1	2.8	3.3	3.7	4.0
Point source placed at the center of AFOV in a 20 cm diam. phantom (B)	1	2.4	2.7	2.8	2.8
Uniform source distribution in a 20 cm diameter phantom (C)	1	10	18	29	46
Uniform source distribution in a 35 cm diameter phantom (C)	1	14	24	38	58

generally achieve similar or higher system sensitivity and, in turn, improved lesion detectability by increasing the scanner axial length instead of crystal thickness [22]. Note that thicker crystals have the drawback of increased parallax error leading to a degradation in system spatial resolution, both transverse and axial. In contrast, extending AFOV promises a bigger advantage for improving PET system sensitivity as opposed to using thicker crystals, even though the overall cost will be higher since such a system will require not only more crystal material but also more photo-sensors.

B. How Long Is Long Enough?

In Fig. 2, we show an illustration of the axial coverage that scanners with an AFOV ranging from 70 to 200 cm will provide for a child and for an average adult male. While TB-PET is clearly achieved with the 200 cm scanner, here, we will use the term TB-PET to refer to a scanner long enough to capture the major organs of the body, approximately 70 cm or longer, depending on the height of the subject.

To be more quantitative about the benefits of TB-PET as a function of AFOV, we show in Fig. 3 the percentage of simulated annihilation events reaching the detector surface as a function of scanner AFOV for varying imaging setups: (A) point source in air placed at the center of the scanner that represents an idealized situation for a single organ imaging without attenuation, (B) point source placed in 200 cm long water-filled, cylindrical phantoms of varying diameters that represents single organ imaging with realistic attenuation, and (C) uniformly distributed source in 200 cm long water-filled, cylindrical phantoms of varying diameters that represents TB imaging with uniform activity together with attenuation. A 20-cm diameter phantom emulates a patient with low body-mass index (BMI), whereas a 40-cm diameter phantom emulates a patient with high BMI. In Setup A, the sensitivity keeps increasing as the scanner axial length increases, but the rate of increase starts to slow beyond 100 cm. In the more realistic Setup B for single organ imaging, the gain in sensitivity is not significant for scanners longer than

100 cm. Finally, for the TB imaging scenario (Setup C), we do see a continued gain in sensitivity as the scanner length increases all the way up to 200 cm. Table I summarizes the expected relative gains in sensitivity for these imaging scenarios for a few representative scanner lengths. A factor of > 40 gain in sensitivity can be expected when imaging patients in a 200 cm long scanner as opposed to a 20 cm long scanner, which potentially can be used to dramatically reduce the dose or scan time. In contrast, the gain for point source (or single organ) imaging with attenuation is more modest (< 3) even for scanners with AFOV of ≥ 100 cm, but should also lead to an improvement in image quality and signal-to-noise.

C. Past Efforts on LAFOV Scanners

While not commercially produced there have been at least two prototype scanners built in the recent past with > 50 cm axial length. One of these systems used BGO crystals and had an axial length of 68.5 cm [23]. However, the system operated in 2-D mode with axial septa leading to reduced sensitivity (∼1% for NEMA measurement, or 2% for a point source). The second system was a fully 3-D prototype developed at Siemens (P39-5H) using LSO crystals and had an axial length of 53 cm [24]. System sensitivity was 2% for NEMA measurement, or 5.3% for a point source. As with the BGO scanner, this LSO scanner also did not operate in TOF mode. Relatively modest gains in image quality, absence of TOF capability, and high cost prevented a transition of these systems into regular clinical use. In recent years, there have been proposals for even longer (100 cm) PET systems using BGO as the scintillator and axial septa that are in-between a fully 3-D and 2-D PET system [25]. While being non-TOF, using BGO together with large conventional PMTs will lead to a cost-effective design of a PET system with sensitivity higher than commercial PET systems while also providing a long AFOV. Operating in a 2-D mode, the sensitivity gain for single organ imaging will not improve, but the longer AFOV will allow an increase in effective sensitivity for whole-body imaging (imaging more of the patient), as well as the ability to perform multiorgan simultaneous dynamic imaging.

D. Current TB-PET Scanners

In 2015, the NIH-funded EXPLORER Consortium was formed to develop a TB-PET scanner with an AFOV long enough to image an adult patient head-to-toe in a single

70 cm   70 cm   140 cm   200 cm
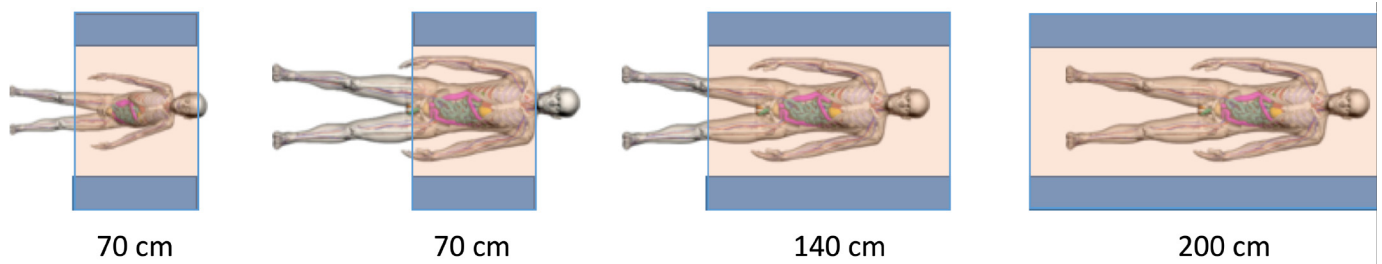
Fig. 2.   Fig. 1: Illustration of axial coverage of a TB-PET scanner of 70 cm, 140 cm, and 200 cm length for an average 6-year child (115 cm (45") tall) and an average adult male (177 cm (70") tall). Images are from the XCAT digital phantoms [26], [27].
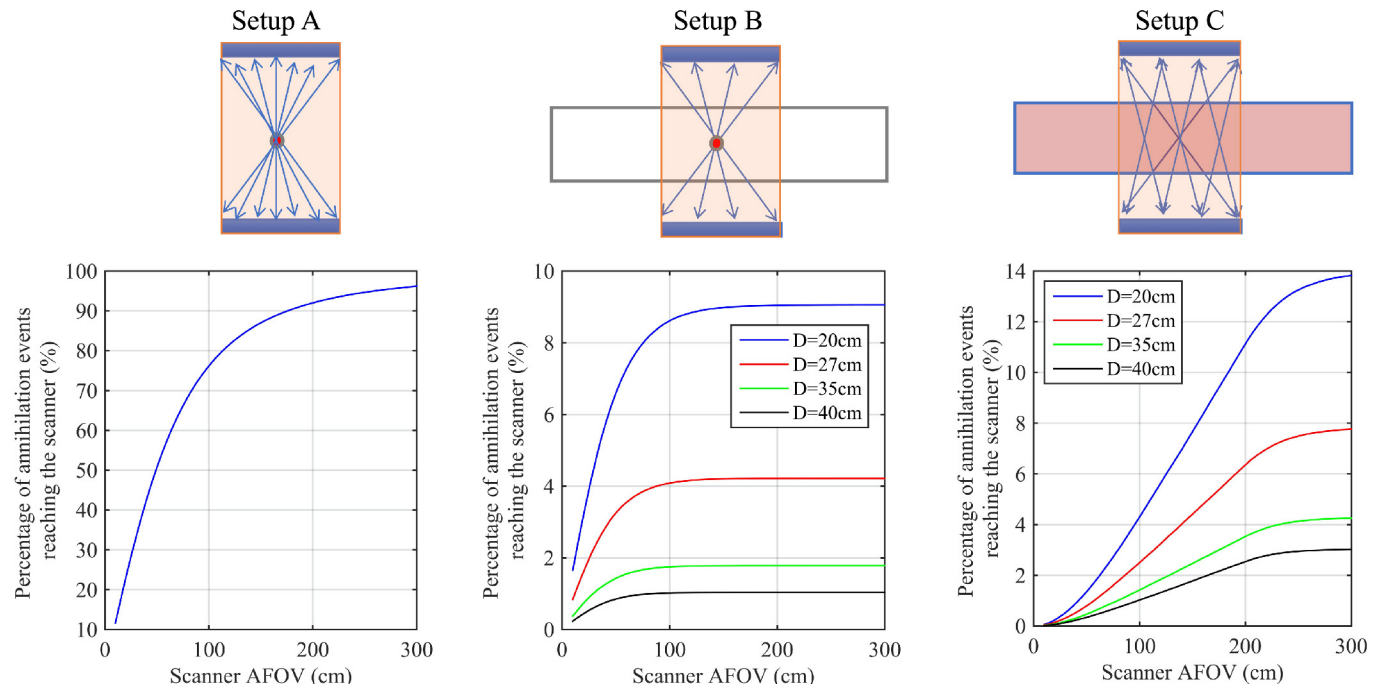

Fig. 3.   Percentage of annihilation events reaching the scanner plotted as a function of scanner AFOV. Three different imaging setups were simulated: Setup A is a point source in air, Setup B is a point source in a 200 cm long water-filled cylinder, and Setup C is a uniformly distributed source in a 200 cm long water-filled cylinder. The cylinder diameter included 20 cm, 27 cm, 35 cm, and 40 cm, representing small to large patients.
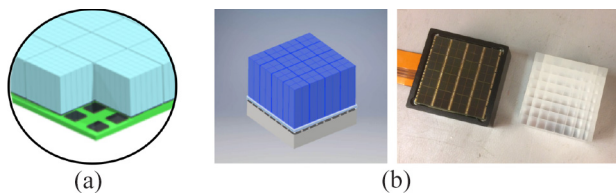

Fig. 4.   Illustration of detectors integrated in current TB-PET scanners. (a) Detector used in uEXPLORER from United Imaging Healthcare with a 7×6 block of LYSO crystals, each $2.76 \times 2.76 \times 18$ mm^3, coupled to 4 SensL SiPMs, each 6-mm^2, thus relying on a light-sharing scheme for crystal identification (courtesy of Dr. Hongdi Li, United Imaging Healthcare America). (b) Detector used in PennPET EXPLORER with an 8×8 block of LYSO crystals, each $3.76 \times 3.76 \times 19$ mm^3, coupled to the PDPC 64-channel digital SiPM in a 1:to:1 scheme for crystal identification [28].

bed position. This project has now resulted in two LAFOV PET scanners, both of which have recently demonstrated their potential in human imaging: the uEXPLORER scanner developed by United Imaging Healthcare (Shanghai, China) in collaboration with the UC Davis team, and the PennPET EXPLORER scanner developed at the University

of Pennsylvania in collaboration with Philips Healthcare (Cleveland, Ohio). Both designs are based on technology also incorporated into commercial scanners with a more standard AFOV. The uEXPLORER scanner uses the same detector as the uMI 550 and 780 PET-CT scanners, while the PennPET EXPLORER uses the same digital tile detector as the Philips Vereos PET-CT scanner. The uEXPLORER scanner is composed of 8 detector rings for a 194 cm total axial FOV and reported to have a spatial resolution of 3.2 mm and CTR of 505 ps, based on NEMA measurements [29]. The detector utilizes a block of 7×6 crystals, each $2.76 \times 2.76 \times 18$ mm^3, coupled to 4 SensL SiPMs, each 6-mm^2 [Fig. 4(a)]. Thus, this detector achieves a $\sim$10:1 crystal:SiPM encoding by relying on a light-sharing technique. The PennPET EXPLORER scanner is based on a scalable design and was initially evaluated in a prototype configuration of 3 rings with gaps between rings leading to an overall axial FOV of 64 cm [30]. The scanner has a spatial resolution of 4.0 mm and CTR of 256 ps. The detector utilizes a block of 8×8 crystal, each $3.76 \times 3.76 \times 19$ mm^3, coupled to the PDPC 64-channel digital SiPM [Fig. 4(b)]. Thus,
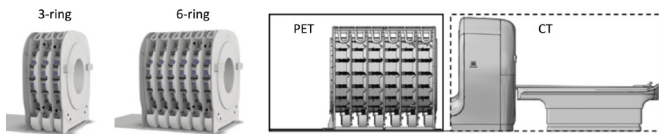
Fig. 5. Illustration of the multiring PennPET EXPLORER scanner. The scalable design, shown in a 3-ring and 6-ring configuration, allows flexibility in building a TB-PET scanner of various axial length. The rings are closely stacked with a small gap of < 1 cm, but can also be separated with a larger gap to extend the axial FOV.

a 1-to-1 crystal:SiPM coupling is achieved, which maximizes the light collection per SiPM and leads to a combination of excellent crystal identification, timing resolution, and minimal deadtime. Compared to the commercial implementation of this detector with the Philips Vereos, the PennPET EXPLORER operates the tile detectors at a lower temperature (5° versus 18°) in order to reduce noise and utilize the trigger 1 level for improved timing performance [30]. The PennPET EXPLORER is being expanded to 6 rings in 2020 that will enable an axial FOV of 140 cm for a wider variety of TB-PET imaging (Fig. 5).

In developing a TB-PET scanner, there were a number of design challenges and choices to be made. First and foremost was deciding upon the axial length. Since the average adult is between 165–175 cm (depending on gender), UC Davis and UIH decided to make their device nearly 2 m to enable total body imaging for nearly all adults. Whether or not it is important to capture the feet simultaneously with the head remains to be seen, although the longer AFOV does preserve high sensitivity for the majority of body. As seen from Fig. 3 the peak sensitivity for a point (or organ) is for an axial length of 100 cm, or less for heavier patients (e.g., > 35-cm diameter). Fig. 6 shows that for a scanner length of 140 cm the sensitivity profile is relatively uniform for the central 80 cm (< 10% change). So, if we want the major organs, from head to pelvis, to be imaged with peak sensitivity, that supports the need for a scanner with > 140-cm total length. Given the uncertainty of the major applications that would be best served by a TB-PET scanner, the choice made for the PennPET EXPLORER was to make it scalable with ring-segments of 23-cm each. As mentioned, this design was first tested with 3 rings (for total 70-cm axial length) and is now being configured with 6 rings (for total 143-cm axial length). In principle more ring-segments can be added (or subtracted), but cost, as well as requirements for planned studies at Penn, were taken into consideration in making this decision. Another practical consideration is room size. While a 2-m long PET scanner may require a room that is larger than normal for PET-CT in a hospital facility, the 1.4-m long PennPET EXPLORER is sited in a room of typical size (20' × 27') for PET-CT where the room length is dictated mainly by the bed travel required for whole-body surveys.

While the axial length determines the sensitivity, assuming that crystal material and thickness are considered constant, there were also considerations about which performance characteristics to prioritize. The uEXPLORER design emphasized improving spatial resolution, while the PennPET EXPLORER design emphasized improving TOF resolution. Of course, both factors contribute to image quality and quantitative accuracy,
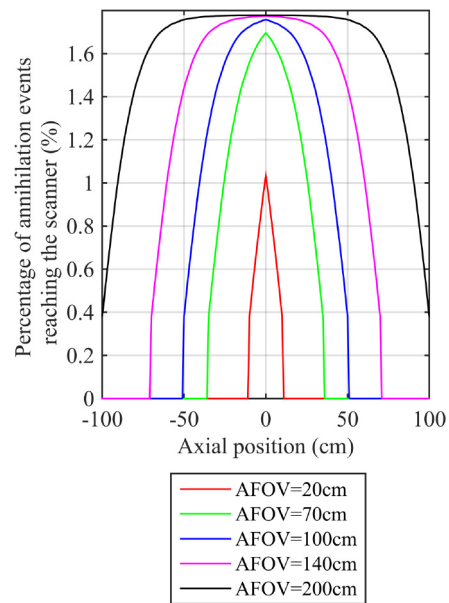

Fig. 6. Axial sensitivity (percentage of events reaching the scanner) profile for a line source in a 35-cm diameter × 200-cm long cylinder, shown for a scanner with 20 cm, 70 cm, 140 cm, and 200 cm AFOV.

and their relative importance for TB-PET imaging will be borne out as more clinically relevant studies are performed. Regardless of design, all TB-PET scanners will collect data sets considerably larger than scanners with standard AFOV, assuming that similar dose and scan time is used. This requires both larger data storage as well as more powerful CPUs or GPUs for image reconstruction. For the uEXPLORER the data are sorted into coincidences in hardware, using a predefined axial acceptance angle (determined by the number of rings in coincidence), whereas the PennPET EXPLORER collects singles event data from each ring in parallel, and performs coincidence sorting in software. Thus, the event throughput is high (maximum 100 Mcps per ring) with little deadtime, even for a study in which a fast bolus is injected. Although the axial acceptance angle can be adjusted, retrospectively, up to the maximum, it is likely that it will be set to a value below the maximum for an average-sized adult since most oblique lines-of-response (LORs) will be attenuated and increasing the acceptance angles will result in increased random coincidences relative to true coincidences. This tradeoff will also depend on optimizing the coincidence window.

Ultimately, the optimal axial length will be determined by the applications, as will the priority of individual design factors that impact on imaging performance. While cost is an important factor, its relative importance depends on whether a TB-PET instrument is used as a clinical instrument to increase patient throughput, or to broaden the scope of research investigations with novel radio-tracers and potentially associated clinical applications. Alternative concepts for TB-PET scanner designs that may either improve performance or make them more cost-effective are discussed in the next section.

E. Alternative TB-PET Scanner Designs

Both of the current TB-PET scanners developed under the EXPLORER Consortium use small cross-section, pixelated

crystals, arranged in a block and coupled to SiPM arrays. An alternative detector option is to use larger, monolithic scintillation detectors that are capable of providing even higher spatial resolution, potentially improved CTR, as well as depth-of-interaction (DOI) measurement capability [31], [32]. Measurements show that such detectors are capable of achieving high sensitivity, spatial resolution < 1.5 mm (FWHM), and a CTR < 150 ps [33]. With a DOI measurement to minimize parallax errors, one could reduce the scanner diameter to maintain system sensitivity while using less crystal—making the system cost-effective and still high performance. A major challenge of monolithic detectors is the complexity of positioning and timing algorithms, which will be increasingly difficult to perform in the high data acquisition rate presents in TB-PET scanners.

Modern PET/CT detectors using pixelated Lu-based scintillators coupled to SiPM arrays can also be used to develop cost-effective LAFOV systems by reducing the total amount of detector present in the scanner. As described above, previous work [22] has shown that system designs using a fixed crystal volume as that used in current commercial PET systems but using thinner crystals (< 20 mm thick) and a longer scanner AFOV can achieve similar or slightly higher system sensitivity, as well as improved clinical performance, such as lesion detectability [34]. Alternatively, there have been proposals for using Lu-based detectors in a sparse arrangement (gaps, axially and/or transaxially) [35]–[40], thereby reducing the detector cost while achieving longer axial FOV coverage. The redundancy of fully 3-D PET together with TOF information provide the ability to reconstruct tomographic images with any detector motion. In fact, the concept of using gaps between detector rings has been tested in the prototype configuration of the PennPET EXPLORER [30], [41] with data gaps in each ring corresponding to a data loss of 30 percent of each ring. These studies demonstrated that high quality, artifact-free images can be generated with such data loss. While the sensitivity of systems using thin crystals or sparse detector arrangement will be lower than current TB-PET scanners, they will provide the ability to perform dynamic whole-body imaging due to their long AFOV.

Finally, a very different design for a cost-effective TB-PET scanner is to use long plastic scintillators along the axial direction [42]. Plastic is very inexpensive and provides a very fast timing signal. Measurement of scintillation photon arrival times at the two ends of a plastic tube provides the axial position of an event within the detector. In addition, for a coincident event in two separate detectors, the arrival times provide the TOF information along the line-of-response as needed for TOF PET. A significant disadvantage of a plastic-based system is the low detection efficiency for 511 keV photons, leading to the need for a thick, or multilayer detector to achieve comparable system sensitivity.

III. CLINICAL AND RESEARCH APPLICATIONS

Initial studies with both the uEXPLORER and the PennPET EXPLORER in humans have demonstrated encouraging early results, representing the successful human translation of these instruments. Several of the proposed benefits of these LAFOV

Fig. 7. Images (reconstructed into 2-mm^3 voxels) of a 170 cm male acquired on the PennPET EXPLORER in its prototype (3-ring) configuration. A dose of 551 MBq (14.9 mCi) was injected and the scan acquired for 20 min at 1.75 h post-injection.

scanners described above have been substantiated. Most easily appreciated, both instruments produce superior image quality compared to commercial PET scanners. These promising early studies have spurred the study of numerous potential applications for these instruments—both in the clinical and research space.

A. Direct Clinical Applications

Both the uEXPLORER and the PennPET EXPLORER produce qualitatively superior images, unmatched by modern standard-of-care clinical scanners. Examples of FDG studies from the PennPET EXPLORER are shown in Figs. 7 and 8. Images on these LAFOV devices reveal low noise and anatomic details not easily appreciated on commercial scanners, including vessel walls and brain substructures [41], [43]. Improvements in imaging quality may have direct clinical application. In a patient with metastatic colon cancer, the PennPET EXPLORER demonstrated better delineation of perihepatic disease, both prior to and after chemotherapy. A better understanding of disease burden, including residual disease, may have direct clinical implications.

The increased sensitivity of the EXPLORER has been leveraged to acquire images of diagnostic image quality with less injected activity than is typically used in the clinic. The uEXPLORER imaged a 43.5 kg, 152 cm female volunteer (BMI = 18.8) with 25 MBq (0.7 mCi) of FDG [43]. The images demonstrated good quality and a normal biodistribution of FDG with a dose ~5% of a typical FDG dose (15 mCi). On the PennPET EXPLORER a 71 kg, 164 cm female volunteer (BMI = 26.4) was injected with 577 MBq (15.5 mCi) and scanned for 20 min at 1.5 h p.i., but the data were subsampled to generate an image with 1/16 of the counts, thus corresponding to a 1.25 min scan or 1 mCi dose. These images shown in Fig. 8(b) demonstrate good quality, similar to the findings from the uEXPLORER study.

On the PennPET EXPLORER, a clinical patient with metastatic neuroendocrine cancer was scanned 3.5 h after her clinical standard-of-care ^{68}Ga-DOTATATE PET-CT [41]. Comparable image quality was achieved, even though the images were obtained with effectively one-fifth of the dose of the clinical scan at the time of scanning [equivalent to injecting ~30 MBq (0.8 mCi)]. Given production issues inherent with ^{68}Ga-DOTATATE, and ongoing efforts to produce this radionuclide with a cyclotron [44], imaging with less injected
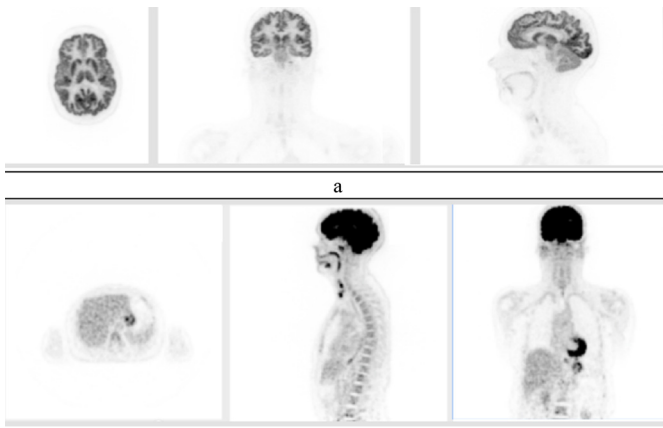
Fig. 8. 164 cm female was scanned on the PennPET EXPLORER in its prototype (3-ring) configuration. A dose of 577 MBq (15.5 mCi) was injected and the scan acquired for 20 min at 1.5 hr post-injection. (a) Data reconstructed into 1-mm^3 voxels show selective images of brain. (b) Data reconstructed into 4-mm^3 voxels, but subsampled with 1/16 the counts, corresponding to a scan time of 1.25 min or a dose of 1 mCi.

activity may enable more patient access. For pediatrics, imaging with lower dose can also decrease radiation risk. By combining a low-injected dose with joint reconstruction algorithms that do not require a CT [45], [46], or with MRI [47], additional gains may be obtained. Finally, low-dose imaging may enable dual-isotope imaging with the same radionuclide, discussed below.

As an alternative to both of the above applications—superior image quality or imaging with less injected activity—these instruments could be utilized to obtain images with a shorter scan duration. Subsampling list-mode data on both the uEX-PLORER and PennPET EXPLORER demonstrated diagnostic quality imaging with scans as short as 1–2 min, and even less [41], [43]. Such short scans could increase patient throughput in a busy clinic. Workflow could become more akin to that of a CT scanner, limited more by patient factors than actual scan time. Short scans of pediatric patients may obviate the need for anesthesia, avoiding risks inherent with the anesthetic, as well as necessary concomitant invasive monitoring [48]. Novel imaging protocols can also be developed to leverage this new ability. For example, quantification of FDG uptake of pulmonary nodules, particularly small nodules at the lung bases, is fraught with error secondary to partial volume effects and respiratory motion artifact. Breath-hold FDG-PET CT with images obtained in ∼30 s or less, as can be achieved with an LAFOV scanner, can mitigate these issues [49], and obviate the need for sophisticated motion-correction algorithms [50].

Analogous to imaging with lesser injected activity, the increased sensitivity of an LAFOV scanner could be leveraged for delayed imaging, with imaging times far beyond what is possible with conventional PET scanners. The uEX-PLORER demonstrated diagnostic-quality imaging in a female volunteer 10 h after the injection of 256 MBq (6.9 mCi) of FDG [43]. Human volunteers were imaged up to 24 h—over 10 half-lives—on the PennPET EXPLORER after the injection of ∼555 MBq (∼15 mCi) of FDG [41]. In this application, differential radiotracer kinetics in tumors versus normal tissues

may be exploited, as opposed to simply imaging with less injected dose. For example, FDG accumulates in tumors over time owing to trapping via the hexokinase enzyme. Tumor contrast increases over time as FDG washes out from normal tissue. As such, delayed imaging may have increased sensitivity for detection of hypermetabolic disease [51]. Delayed imaging has particular promise in detection of liver metastases as metastases are variably hypermetabolic and the liver has high background activity that decreases over time [52]. Combining delayed imaging with novel radiotracers, including long-lived isotopes, should allow an extended study of *in vivo* biology as further discussed in the following section.

B. Research Applications

Beyond direct clinical applications, the increased sensitivity of an LAFOV scanner and the ability to image all major organs simultaneously has profound research implications. The wide range of potential research applications for such modern LAFOV scanners helped to justify the actual construction of the instruments [53]. In the short time since construction of the uEXPLORER and PennPET EXPLORER, the research potential of these devices has started to materialize. The following examples highlight some notable early research studies on these scanners. Examples of such future studies likely to be performed at Penn are also discussed.

These applications span a wide range of complexity, from static imaging with known radiotracers to whole-body dynamic studies of novel agents. The ability to capture relatively noise-free time activity in multiple organs and lesions enhances our ability to study radiotracer kinetics. Dynamic imaging on the PennPET EXPLORER and uEXPLORER demonstrated blood input functions with low sampling noise [41], [43]. As the radiotracer bolus traveled through the vasculature, the arterial input curves demonstrated progressively blunted peaks secondary to dispersion and partial volume averaging [41], [54], underscoring the variability of available arterial input functions for kinetic model selection. Imaging with a long AFOV scanner ensures the field-of-view always contains a large vascular structure for an input function, possibly eliminating some of the need for sophisticated correction techniques [55]. Moreover, imaging the entire body will not limit an investigator to select an anatomic area for dynamic coverage. An LAFOV scanner will capture all lesions, and combined with kinetic analysis would mainstream whole-body parametric imaging [56], which in turn will enable a more complete characterization of disease burden across an entire patient. An example of the quality of dynamic imaging with such devices is shown in Fig. 9. Given known associations of tumoral heterogeneity and resistance to targeted therapy [57], such information could inform treatment.

Superior image quality of the brain, as demonstrated on the PennPET EXPLORER with delineation basal ganglia subregions [41], can be leveraged for studying these structures with known pathology in neurologic diseases. FDG-PET studies to localize subtle foci of hypometabolism indicative of seizure foci can also be undertaken. But, what is unique about an LAFOV scanner is the inclusion of all organs in a single field-of-view that enables novel approaches to study
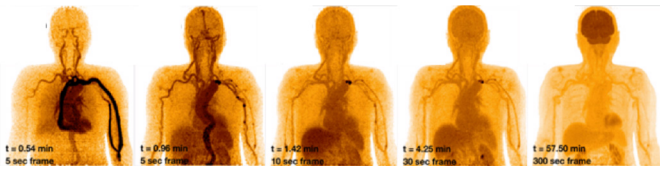
Fig. 9. Example of dynamic study acquired on PennPET EXPLORER in its prototype (3-ring) configuration, illustrating ability to measure whole-body kinetics. Five representative frames, from 5 s to 5 min duration, are shown over the course of 1 h, following injection of 15 mCi FDG.

the physiologic or pathophysiological interactions between organs, including brain-body interactions. For example, the endogenous opioid system, implicated in the pathophysiology of drug addiction, includes both central and peripheral nervous system components. Exogenous opiate consumption use often has widespread effects on this system, e.g., constipation and respiratory depression peripherally and sedation centrally [58]. Radiotracers have been developed to image the opioid receptor, such as ^{11}C-carfentanil, a μ-opioid receptor agonist [59]. Imaging on conventional scanners, though, captures the brain at the exclusion of the spinal cord and peripheral nervous system. The LAFOV scanner will allow studies of interactions across the entire opioid system. These studies could be used to develop new opiate-receptor targeting drugs that bind differentially to central and peripheral system receptors which, in turn, may confer lower abuse potential.

The superior sensitivity of the LAFOV scanner can be utilized to image radioisotopes with low positron abundance, including ^{90}Y and ^{89}Zr with positron abundance of 0.0032% and 23%, respectively, [60]. Imaging the rare positron emission of ^{90}Y with PET would allow dosimetry estimates after radioembolization of hepatic tumors with a goal of predicting outcome [61]. Imaging ^{89}Zr with a 3.27-day half-life could enable extended cell-tracking studies. A recent study with the mini-EXPLORER, a 45 cm AFOV scanner designed for primate imaging at UC Davis, imaged ^{89}Zr-labeled antibodies up to 30 days after injection in rhesus monkeys. Changes in tracer biodistribution were appreciated over ∼9 half-lives of ^{89}Zr [62]. In humans, a recent clinical trial studied a radiolabeled minibody against CD8+ T cell,^{89}Zr-IAB22M2C, in tracking these immune cells involved in the response to immunotherapy. With conventional scanners, images were obtained up to 144 h post-injection [63]. Imaging with the LAFOV scanner would enable more delayed imaging and tracking.

Finally, the sensitivity of the LAFOV scanner may permit dual-tracer PET imaging, allowing the *in vivo* interrogation of two distinct biologic processes in the same imaging session. On current modern scanners, this necessitates two days of imaging to allow sufficient tracer decay between injections. To query tumor metabolism, both FDG and ^{18}F-Fluoroglutamine, a radiotracer of glutamine metabolism [64], [65], can be studied in immediate succession. Such a study is being planned on the PennPET EXPLORER. A relatively low dose of ^{18}F-Fluoroglutamine will be imaged first, exploiting the superior sensitivity of LAFOV PET scanner. The volume of distribution and delivery of ^{18}F-Fluoroglutamine can be calculated from

kinetic analysis of 30 min of dynamic imaging. Subsequently, a greater dose of FDG will be injected and dynamic imaging will continue unabated. Kinetic image analysis of FDG could yield delivery and flux estimates, with the analysis accounting for residual ^{18}F-Fluoroglutamine. Ultimately, in 1.5 h, kinetic parameters of tumor glutamine and glucose metabolism could be estimated [66]. Other tracer pairs are also possible—e.g., FDG and ^{68}Ga-DOTATATE—enhancing the ability of PET to characterize tumor biology to inform treatment.

IV. CONCLUSION

Encouraging early studies of the EXPLORER scanners at UC Davis and Penn have substantiated the benefits of a TB-PET scanner in both clinical and research applications. In certain practice settings, an LAFOV scanner could benefit routine clinical care when the high sensitivity is appropriately leveraged, e.g., injecting a lesser activity for pediatric patients or for a radiotracer in limited supply, or faster scans to increase throughput in a busy clinical practice. The large axial coverage enables dynamic studies that are impossible to perform with a standard axial FOV.

With such versatility of TB-PET, we believe more vendors will develop LAFOV scanners. Even though FDG imaging will almost certainly continue to be the primary clinical application, which is well served by scanners with a standard AFOV, we believe that there is an important role for LAFOV scanners to play. Ultimately marketing and cost considerations, rather than technology limitations, will determine how many LAFOV scanners are produced and how quickly TB-PET becomes widely accepted. While there may be advantages to develop such scanners with novel technology, it is more likely that for the near future the vendors will leverage existing technology from commercial PET-CT with standard AFOV, as the uEXPLORER and PennPET EXPLORER have done. To balance cost-effectiveness and benefit, the axial FOV of such scanners may not need to cover the entire body; an axial FOV of ∼1 m may be ideal. When appropriately matched with clinical or research indications, we believe these powerful scanners have the potential to transform PET research and patient care.

REFERENCES

[1] A. R. Pantel, D. Ackerman, S.-C. Lee, D. A. Mankoff, and T. P. Gade, "Imaging cancer metabolism: Underlying biology and emerging strategies," *J. Nucl. Med.*, vol. 59, no. 9, pp. 1340–1349, Sep. 2018.

[2] B. C. Uzuegbunam, D. Librizzi, and B. H. Yousefi, "PET radiopharmaceuticals for alzheimer's disease and parkinson's disease diagnosis, the current and future landscape," *Molecules*, vol. 25, no. 4, p. E977, 2020.

[3] E. E. Parent and D. M. Schuster, "Update on ^{18}F-fluciclovine PET for prostate cancer imaging," *J. Nucl. Med.*, vol. 59, no. 5, pp. 733–739, May 2018.

[4] T. F. Budinger, "PET instrumentation: What are the limits?" *Seminars Nucl. Med.*, vol. 28, no. 3, pp. 247–267, 1998.

[5] M. E. Casey and R. Nutt, "A multicrystal two dimensional BGO detector system for positron emission tomography," *IEEE Trans. Nucl. Sci.*, vol. 33, no. 1, pp. 460–463, Feb. 1986.

[6] G. Muehllehner, M. P. Buchin, and J. H. Dudek, "Performance parameters of a positron imaging camera," *IEEE Trans. Nucl. Sci.*, vol. 23, no. 1, pp. 528–537, Feb. 1976.

[7] J. S. Karp et al., "Continuous-slice PENN-PET: A positron tomograph with volume imaging capability," *J. Nucl. Med.*, vol. 31, pp. 617–627, May 1990.

[8] J. S. Karp, G. Muehllehner, M. J. Geagan, and R. Freifelder, "Whole-body PET scanner using curve-plate NaI(Tl) detectors," *J. Nucl. Med.*, vol. 39, no. 5, p. 50, May 1998.

[9] L. E. Adam, J. S. Karp, M. E. Daube-Witherspoon, and R. J. Smith, "Performance of a whole-body PET scanner using curve-plate NaI(Tl) detectors," *J. Nucl. Med.*, vol. 42, no. 12, pp. 1821–1830, Dec. 2001.

[10] T. K. Lewellen, "Time-of-flight PET," *Seminar Nucl. Med.*, vol. 28, no. 3, pp. 268–275, 1998.

[11] D. L. Snyder, L. J. Thomas, and M. M. Ter-Pogossian, "A matheematical model for positron-emission tomography systems having time-of-flight measurements," *IEEE Trans. Nucl. Sci.*, vol. 28, no. 3, pp. 3575–3583, Jun. 1981.

[12] T. F. Budinger, "Time-of-flight positron emission tomography: Status relative to conventional PET," *J. Nucl. Med.*, vol. 24, no. 1, pp. 73–76, 1983.

[13] C. L. Melcher and J. S. Schweitzer, "Cerium-doped lutetium oxyorthosilicate: A fast, efficient new scintillator," *IEEE Trans. Nucl. Sci.*, vol. 39, no. 4, pp. 502–505, Aug. 1992.

[14] S. Surti, A. Kuhn, M. E. Werner, A. E. Perkins, J. Kolthammer, and J. S. Karp, "Performance of Philips Gemini TF PET/CT scanner with special consideration for its time-of-flight imaging capabilities," *J. Nucl. Med.*, vol. 48, no. 3, pp. 471–480, 2007.

[15] S. Surti and J. S. Karp, "Advances in time-of-flight PET," *Physica Medica*, vol. 32, pp. 12–22, Jan. 2016.

[16] K. Wienhard et al., "The ECAT EXACT HR: Performance of a new high resolution positron scanner," *J. Comput. Assist. Tomography*, vol. 18, no. 1, pp. 110–118, 1994.

[17] T. J. Spinks et al., "Physical characteristics of the ECAT EXACT3D positron tomograph," *Phys. Med. Biol.*, vol. 45, no. 9, pp. 2601–2618, Sep. 2000.

[18] J. Zhang, P. Maniawski, and M. V. Knopp, "Performance evaluation of the next generation solid-state digital photon counting PET/CT system," *EJNMMI Res.*, vol. 8, no. 1, p. 97, Nov. 2018.

[19] T. Pan et al., "Performance evaluation of the 5-Ring GE discovery MI PET/CT system using the national electrical manufacturers association NU 2-2012 standard," *Med. Phys.*, vol. 46, no. 7, pp. 3025–3033, 2019.

[20] J. van Sluis et al., "Performance characteristics of the digital biograph vision PET/CT system," *J. Nucl. Med.*, vol. 60, no. 7, pp. 1031–1036, 2019.

[21] K. Nakanishi, Y. Hirano, and S. Yamamoto, "Comparison of noise equivalent count rates (NECRs) for the PET systems with different ring diameter and electronics," *IEEE Trans. Radiat. Plasma Med. Sci.*, vol. 3, no. 3, pp. 371–376, May 2019.

[22] S. Surti, M. E. Werner, and J. S. Karp, "Study of PET scanner designs using clinical metrics to optimize the scanner axial FOV and crystal thickness," *Phys. Med. Biol.*, vol. 58, pp. 3995–4012, Jun. 2013.

[23] M. Watanabe et al., "A high-throughput whole-body PET scanner using flat panel PS-PMTs," *IEEE Trans. Nucl. Sci.*, vol. 51, no. 3, pp. 796–800, Jun. 2004.

[24] M. Conti et al., "Performance of a high sensitivity PET scanner based on LSO panel detectors," *IEEE Trans. Nucl. Sci.*, vol. 53, no. 3, pp. 1136–1142, Jun. 2006.

[25] Y. Zhang and W. H. Wong, "System design studies for a low-cost high-resolution BGO PET with 1-meter axial field of view," *J. Nucl. Med.*, vol. 58, p. 221, May 2017.

[26] W. P. Segars, G. Sturgeon, S. Mendonca, J. Grimes, and B. M. W. Tsui, "4D XCAT phantom for multimodality imaging research," *Med. Phys.*, vol. 37, no. 9, pp. 4902–4915, 2010.

[27] W. Kainz et al., "Advances in computational human phantoms and their applications in biomedical engineering—A topical review," *IEEE Trans. Radiat. Plasma Med. Sci.*, vol. 3, no. 1, pp. 1–23, Jan. 2019.

[28] C. Degenhardt et al., "The digital Silicon photomultiplier—A novel sensor for the detection of scintillation light," in *Proc. IEEE Nucl. Sci. Symp. Med. Imag. Conf.*, Orlando, FL, USA, 2009, pp. 2383–2386.

[29] B. A. Spencer et al., "Performance evaluation of the EXPLORER total-body PET/CT scanner based on NEMA NU-2 2018 standard with additional tests for extended geometry," in *Proc. IEEE Nucl. Sci. Symp. Med. Imag. Conf.*, Manchester, U.K., 2019, p. M07-03.

[30] J. S. Karp et al., "PennPET explorer: Design and preliminary performance of a whole-body imager," *J. Nucl. Med.*, vol. 61, pp. 136–143, Jan. 2020.

[31] H. T. van Dam, G. Borghi, S. Seifert, and D. R. Schaart, "Sub-200 ps CRT in monolithic scintillator PET detectors using digital SiPM arrays and maximum likelihood interaction time estimation," *Phys. Med. Biol.*, vol. 58, no. 10, pp. 3243–3258, 2013.

[32] S. Seifert, G. van der Lei, H. T. van Dam, and D. R. Schaart, "First characterization of a digital SiPM based time-of-flight PET detector with 1 mm spatial resolution," *Phys. Med. Biol.*, vol. 58, no. 9, pp. 3061–3074, 2013.

[33] G. Borghi, B. J. Peet, V. Tabacchini, and D. R. Schaart, "A 32 mm × 32 mm × 22 mm monolithic LYSO: Ce detector with dual-sided digital photon counter readout for ultrahigh-performance TOF-PET and TOF-PET/MRI," *Phys. Med. Biol.*, vol. 61, no. 13, pp. 4929–4949, 2016.

[34] V. Viswanath, M. E. Daube-Witherspoon, J. S. Karp, and S. Surti, "Numerical observer study of lesion detectability for a long axial field-of-view whole-body PET imager using the PennPET explorer," *Phys. Med. Biol.*, vol. 65, Jan. 2020, Art. no. 035002.

[35] T. Yamaya et al., "A proposal of an open PET geometry," *Phys. Med. Biol.*, vol. 53, no. 3, pp. 757–773, 2008.

[36] J. Zhang, M. I. Knopp, and M. V. Knopp, "Sparse detector configuration in SiPM digital photon counting PET: A feasibility study," *Mol. Imag. Biol.*, vol. 21, no. 3, pp. 447–453, Jun. 2019.

[37] N. A. Karakatsanis, S. A. Zein, and S. A. Nehmeh, "Evaluation of image quality and quantitation in a clinical PET scanner with a uniformly sparse detector rings configuration," in *Proc. IEEE Nucl. Sci. Symp. Med. Imag. Conf. (NSS/MIC)*, Sydney NSW, Australia, Nov. 2018, pp. 1–9.

[38] S. Vandenberghe, "PET 20.0: A cost-efficient, 2mm spatial resolution total body PET with point sensitivity up to 22% and adaptive axial FOV of maximum 2.00m," *Eur. J. Nucl. Med. Mol. Imag.*, vol. 44, no. 2, p. S305, 2017.

[39] Z. Zhang et al., "Preliminary investigation of optimization-based image reconstruction for TOF PET with sparse configurations," in *Proc. 15th Int. Meeting Fully Three Dimensional Image Reconstr. Radiol. Nucl. Med.*, Philadelphia, PA, USA, 2019, Art. no. 110720L.

[40] M. E. Daube-Witherspoon, V. Viswanath, S. Surti, and J. S. Karp, "Reconstruction performance for long axial field-of-view PET scanners with large axial gaps," in *Proc. 15th Int. Meeting Fully Three Dimensional Image Reconstr. Radiol. Nucl. Med.*, Philadelphia, PA, USA, 2019, Art. no. 110722C.

[41] A. R. Pantel et al., "PennPET explorer: Human imaging on a whole-body imager," *J. Nucl. Med.*, vol. 61, pp. 144–151, Jan. 2020.

[42] P. Moskal et al., "Time resolution of the plastic scintillator strips with matrix photomultiplier readout for J-PET tomograph," *Phys. Med. Biol.*, vol. 61, no. 5, pp. 2025–2047, Feb. 2016.

[43] R. D. Badawi et al., "First human imaging studies with the EXPLORER total-body PET scanner," *J. Nucl. Med.*, vol. 60, no. 3, pp. 299–303, 2019.

[44] W. Tieu et al., "Rapid and automated production of [^{68}Ga]gallium chloride and [^{68}Ga]Ga-DOTA-TATE on a medical cyclotron," *Nucl. Med. Biol.*, vols. 74–75, pp. 12–18, Jul./Aug. 2019.

[45] A. Rezaei, M. Defrise, and J. Nuyts, "ML-reconstruction for TOF-PET with simultaneous estimation of the attenuation factors," *IEEE Trans. Med. Imag.*, vol. 33, no. 7, pp. 1563–1572, Jul. 2014.

[46] J. Nuyts, A. Rezaei, and M. Defrise, "The validation problem of joint emission/transmission reconstruction from TOF-PET projections," *IEEE Trans. Radiat. Plasma Med. Sci.*, vol. 2, no. 4, pp. 273–278, Jul. 2018.

[47] N. S. Kwatra, R. Lim, M. S. Gee, L. J. States, A. Vossough, and E. Y. Lee, "PET/MR Imaging:: Current Updates on Pediatric Applications," *Mag. Resonance Imag. Clin. North Amer.*, vol. 27, no. 2, pp. 387–407, 2019.

[48] B. L. Shulkin, "PET imaging in pediatric oncology," *Pediatric Radiol.*, vol. 34, no. 3, pp. 199–204, Mar. 2004.

[49] T. Torizuka *et al.*, "Single 20-second acquisition of deep-inspiration breath-hold PET/CT: Clinical feasibility for lung cancer," *J. Nucl. Med.*, vol. 50, no. 10, pp. 1579–84, Oct. 2009.

[50] Y. Lu *et al.*, "Respiratory motion compensation for PET/CT with motion information derived from matched attenuation-corrected gated PET data," *J. Nucl. Med.*, vol. 59, no. 9, pp. 1480–1486, Sep. 2018.

[51] K. Kubota *et al.*, "Advantage of delayed whole-body FDG-PET imaging for tumour detection," *Eur. J. Nucl. Med.*, vol. 28, no. 6, pp. 696–703, Jun. 2001.

[52] J. W. Lee, S. K. Kim, S. M. Lee, S. H. Moon, and T. S. Kim, "Detection of hepatic metastases using dual-time-point FDG PET/CT scans in patients with colorectal cancer," *Mol. Imag. Biol.*, vol. 13, no. 3, pp. 565–572, Jun. 2011.

[53] S. R. Cherry, R. D. Badawi, J. S. Karp, W. W. Moses, P. Price, and T. Jones, "Total-body imaging: Transforming the role of positron emission tomography," *Sci. Transl. Med.*, vol. 9, no. 381, 2017, Art. no. eaaf6169.

[54] X. Zhang *et al.*, "Total-body dynamic reconstruction and parametric imaging on the uEXPLORER," *J. Nucl. Med.*, vol. 61, no. 2, pp. 285–291, Feb. 2020.

[55] P. Zanotti-Fregonara, K. Chen, J. S. Liow, M. Fujita, and R. B. Innis, "Image-derived input function for brain PET studies: Many challenges and few opportunities," *J. Cerebr. Blood Flow Metab.*, vol. 31, no. 10, pp. 1986–98, Oct. 2011.

[56] J. Gallezot, Y. Lu, M. Naganawa, and R. E. Carson, "Parametric imaging with PET and SPECT," *IEEE Trans. Radiat. Plasma Med. Sci.*, vol. 4, no. 1, pp. 1–23, Jan. 2020.

[57] I. Dagogo-Jack and A. T. Shaw, "Tumour heterogeneity and resistance to cancer therapies," *Nat. Rev. Clin. Oncol.*, vol. 15, no. 2, pp. 81–94, Feb. 2018.

[58] E. E. Benarroch, "Endogenous opioid systems: Current concepts and clinical correlations," *Neurology*, vol. 79, no. 8, pp. 807–14, Aug. 2012.

[59] L. Nummenmaa *et al.*, "μ -opioid receptor system mediates reward processing in humans," *Nat. Commun.*, vol. 9, no. 1, p. 1500, Apr. 2018.

[60] M. Conti and L. Eriksson, "Physics of pure and non-pure positron emitters for PET: A review and a discussion," *EJNMMI Phys.*, vol. 3, no. 1, p. 8, Dec. 2016.

[61] M. D'Arienzo *et al.*, "90Y PET-based dosimetry after selective internal radiotherapy treatments," *Nucl. Med. Commun.*, vol. 33, no. 6, pp. 633–40, Jun. 2012.

[62] E. Berg *et al.*, "Total-body PET and highly stable chelators together enable meaningful ^{89}Zr-antibody PET studies up to 30 days after injection," *J. Nucl. Med.*, vol. 61, no. 3, pp. 453–460, Mar. 2020.

[63] N. Pandit-Taskar *et al.*, "First-in-human imaging with ^{89}Zr-Df-IAB22M2C anti-CD8 minibody in patients with solid malignancies: Preliminary pharmacokinetics, biodistribution, and lesion targeting," *J. Nucl. Med.*, vol. 61, pp. 512–519, Apr. 2020.

[64] B. P. Lieberman *et al.*, "PET imaging of glutaminolysis in tumors by 18F-(2S,4R)4-fluoroglutamine," *J. Nucl. Med.*, vol. 52, no. 12, pp. 1947–55, Dec. 2011.

[65] R. Zhou *et al.*, "[^{18}F](2S,4R)4-fluoroglutamine PET detects glutamine pool size changes in triple-negative breast cancer in response to glutaminase inhibition," *Cancer Res.*, vol. 77, no. 6, pp. 1476–1484, Mar. 2017.

[66] D. A. Mankoff, A. R. Pantel, V. Viswanath, and J. S. Karp, "Advances in PET diagnostics for guiding targeted cancer therapy and studying in Vivo cancer biology," *Current Pathobiol. Rep.*, vol. 7, no. 3, pp. 97–108, 2019.